

# A 4T Superconducting Wiggler for the ESRF

M. Stampfer\*, P. Elleaume  
European Synchrotron Radiation Facility  
BP 220  
Grenoble, France

## Abstract

The magnetic and thermal characteristics of the 4T superconducting wiggler planned for installation in the ESRF storage ring in Fall 1994 are presented. The warm bore superconducting wiggler has a design critical energy of 100keV. The wiggler manufacture is to be carried out in industry by SIEMENS in Bergisch Gladbach, Germany. Characteristics of the coil geometry and field intensity as well as thermal load calculations on the wiggler cryostat are presented. Radiation spectrum calculations and linear and non-linear effects on the e- beam are studied and presented.

## 1 INTRODUCTION

A superconducting wavelength shifter with a nominal field of 4T will be commissioned in the high energy scattering beamline (ID15) of the ESRF. The design and manufacture of the wavelength shifter is being carried out in industry at SIEMENS AG in Bergisch Gladbach, Germany in cooperation with a parallel design carried out at the ESRF. The principle design rules set out for the magnetic design of the superconducting wiggler are as follows:

- An alternating negative/positive/negative vertical magnetic field with a peak value on axis  $B_0 > 4T$ .
- The net field integral along the electron beam axis over the positive central region of the magnet is not to exceed 0.256Tm.
- The maximum contribution from each term of the multipole expansion of the field integral at a distance of 25mm horizontally from the central axis must not exceed the following values:

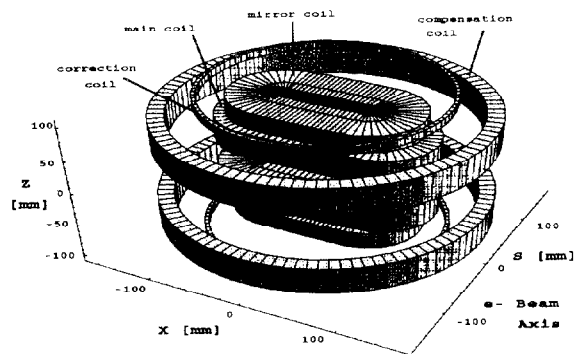
Maximum Field Integrals	
Quadrupole	< 5 [Tmm]
Sextupole	< 10 [Tmm]
Octupole	< 6 [Tmm]
Decapole	< 20 [Tmm]

## 2 MAGNETIC DESIGN

The coil system consists of two pairs of racetrack coils located symmetrically above and below the central axis. The racetrack coils are powered in series with two solenoidal

\*This author wishes to acknowledge the financial support of the EPAC94 local organizing committee.

compensation coils which act to correct for the nonzero field integral occurring on axis. Additional flexibility in field shaping is obtained by additional low current windings on top of the compensation coils which enable fine tuning of the field integral. Each racetrack consists of an inner and outer coil wound with conductor of different dimensions. The inner racetrack coils are wound with 1mm diameter conductor and both the outer coils and circular compensation coils use 0.7mm diameter wire giving overall current densities of 160A/mm<sup>2</sup>, 320A/mm<sup>2</sup> and 160A/mm<sup>2</sup> in the inner, outer and compensation coils respectively.



Coil geometry of the 4T wiggler

The attractive forces between the coils are compensated by a set of active mirror racetrack coils placed above the main coils. The use of active coils simplifies the design by eliminating the use of iron thereby reducing the cold mass of the coil system. The coils are powered in series so as to limit the number of current leads entering into 4K to one pair plus a second pair of low power current leads to power the supplementary windings on the compensation coil. The main racetrack coils are thicker (vertically) and are 15mm longer than the mirror coils in order to reduce the peak field in the racetrack coil heads.

## 3 CRYOGENIC SYSTEM

The cryostat consists of a vertical cylindrical liquid helium tank which contains the coil assembly at its base and the Gifford-MacMahon cold heads in the upper portion of the cylinder. The vertical system has the advantage that the superconducting coils are located in the helium bath below the large reservoir of liquid helium thus allowing a large safety margin in case of refrigerator failure. The cryocooler is a commercial 4.2K closed cycle refrigerator of the

type used frequently for fullbody MRI magnets available from Air Products Division designated HR10-S. It consists of a two stage Gifford-McMahon expander with a Joule-Thompson third stage. The refrigerator is mounted in the flexible neck of the cryostat allowing thermal contact of the cold stations to copper interface blocks in the bellows support. The minimum refrigeration powers of each of the three stages are 30W, 3W and 0.8W at 65K, 18K and 4.3K respectively. Four water cooled compressors with a total output of 10.5kW power the refrigerator. Two copper radiation shields are used at 80K and 20K. An epoxy fiber support post identical to those used in the SSC quadrupole magnet prototypes takes the weight of the magnet coil assembly and simultaneously provide a mounting platform for the radiation shields. Ten layers of superinsulation are used between the radiation shields and thirty layers between the outer radiation shield and the vacuum container. The refrigerator mounts directly into the neck tube of the cryostat and is designed to be removable from the cryostat in case of failure without the need for breaking the insulating vacuum or to warm up the cryostat thereby allowing simplified liquid helium handling and serviceability.

The current leads are non-vapor cooled type made of Aluminum 5083, two of which are thermally anchored to the refrigerator connections. The third stage of the current leads running from 4K to 18K with a length of approximately 15cm consists of rigid bars of high temperature Bi<sub>2</sub>Sr<sub>2</sub> superconductor with a Cu to superconductor ratio of about 7:1. [1]

### 3.1 Heat leak through cryostat parts

The current leads are the dominant source of heat load in the cryostat. Since the wiggler magnet is in persistent current mode under normal operating conditions except during ramping of the magnet, the majority of the heat load from the current leads is due to the thermal conduction from room temperature. An additional contribution to the heat load comes from the small current leads powering the correction coils. These leads are also thermally anchored to the refrigerator cold heads, thereby minimizing the contribution at the 4K level.

### 3.2 Thermal Budget

The total heat load of the cryostat parts and current leads with the current leads unpowered is summarized in the following table.

$I_0=0A$	80K-300K	18K-80K	4K-18K
Heat Shields [W]	15.70	0.05	0.00
Beam Tube [W]	0.03	0.00	0.00
Support Post [W]	3.16	0.48	0.032
Current Leads [W]	6.46	0.83	0.226
Total [W]	25.4	1.36	0.258

Table 1 Heat load during normal operation.

The refrigerator output power at each stage determines the margin for helium loss under normal operating condi-

tions. The following table summarizes the margins under unpowered conditions.

	Ref. Output	$I_0 = 120A$	Factor
80K-300K	30.0 W	25.4 W	1.2
18K-80K	3.0 W	1.36 W	2.2
4K-18K	0.8 W	0.26 W	3.1

Table 2 Safety margins on the refrigerator output power at each cold station .

## 4 EFFECTS ON THE ELECTRON BEAM

The wiggler magnet in the storage ring lattice gives rise to a finite angular focusing and closed orbit displacement of the beam. The angular focusing gives rise to tune shifts which are of importance in the operation of the storage ring as they may excite resonances reducing the lifetime as well as inducing beam size changes which affect the brilliance of the x-ray photon beams seen by users.

The angular and closed orbit displacement can be described by a perturbation expansion of the Lorentz force equation in the inverse of the electron energy [2]. The expansion is done assuming the displacement of an electron is relative to the longitudinal axis defined by an electron moving in a straight line from the initial point of injection.

### 4.1 First order effects

To first order in the inverse of the electron energy, the net angular kicks and closed orbit displacement are given by the integral of the vertical field and double field integral along the longitudinal coordinate. By careful tuning of the current in the circular correction coils, vertical field integrals can be made arbitrarily small. When the condition of zero field integral is fulfilled, the net angle and displacement are zero to first order.

### 4.2 Second order effects

To second order in the inverse of the electron energy, the wiggler field generates horizontal defocusing and vertical focusing on electrons entering off axis. For an electron entering on axis, the net angular displacement is zero to second order by the planer symmetry of the wiggler. In general, the net horizontal and vertical angular displacements can be shown to obey the following equations to second order [3],

$$x_2' = \frac{\partial \Phi}{\partial x} + x_1 \frac{\partial x_1'}{\partial x} + z_1 \frac{\partial z_1'}{\partial x} \quad (1)$$

$$z_2' = \frac{\partial \Phi}{\partial z} + x_1 \frac{\partial x_1'}{\partial z} + z_1 \frac{\partial z_1'}{\partial z}, \quad (2)$$

where  $x_1$  ( $z_1$ ) is the net horizontal (vertical) displacement to first order and  $x_1'$  ( $z_1'$ ) is the net horizontal (vertical) angle to first order and the potential  $\Phi$  is given by,

$$\Phi = -\frac{\alpha^2}{2} \int_{-\infty}^{\infty} [B_x(s)^2 + B_z(s)^2] ds, \quad (3)$$

$$\text{and } \overline{B(s)} = \int_{-\infty}^s B(s') ds', \quad (4)$$

is the field integral along longitudinal coordinate  $s$  and  $\alpha = 0.3/E[\text{GeV}]$ . Assuming overall zero field integrals and double field integrals in both planes, from (1) and (2), the horizontal and vertical focal lengths are given by,

$$\frac{1}{F_x} = \frac{\partial^2 \Phi}{\partial x^2}, \quad \frac{1}{F_z} = \frac{\partial^2 \Phi}{\partial z^2}. \quad (5)$$

To second order in the inverse of the electron energy, the focal lengths are  $5.74 \times 10^{-4} \text{m}^{-1}$  and  $-5.05 \times 10^{-3} \text{m}^{-1}$  in the horizontal and vertical planes respectively. The tune shifts computed at  $\tilde{\beta}_x = 4.70 \text{m}$  and  $\tilde{\beta}_z = 4.46 \text{m}$  are  $-2.15 \times 10^{-4}$  and  $1.99 \times 10^{-3}$  in the horizontal and vertical planes respectively.

## 5 RADIATION SPECTRUM

### 5.1 Radiated Power

For a 6GeV beam of 100mA the total power generated by the wiggler is 5.12kW. The power radiated per horizontal angle is found by summing the field from each source point as an incoherent contribution to the net power, Figure 1 shows the radiated power generated by the wiggler per horizontal angle. The bump seen in the angular power near the central axis is due to the additional flux from the two source points at 0.6T vertical field.

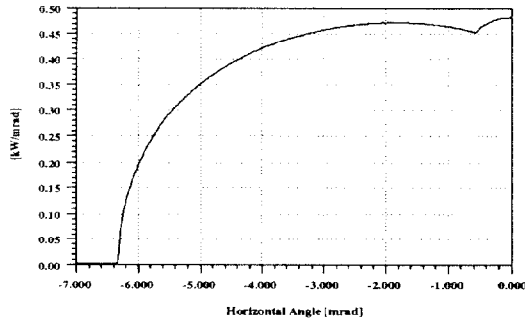


Figure 1: Power integrated in the vertical plane as a function of horizontal angle

### 5.2 Spectral Flux

The angular distribution of the total radiation is given by the averaged intensities of the electric field components in the horizontal (“ $\pi$ -mode”) and vertical (“ $\sigma$ -mode”) polarization directions. The critical energy given by  $\epsilon_c = 3\hbar\gamma^2 c^2 B / 2E_0$  is 95.9keV where  $\hbar$  is Planck’s constant divided by  $2\pi$ . The corresponding critical wavelength is  $\lambda_c = 0.129 \text{\AA}$ . Figure 2 shows the flux as a function of horizontal angle at four photon energies corresponding to  $\frac{\epsilon}{\epsilon_c} = 0.33$ ,  $\frac{\epsilon}{\epsilon_c} = 0.66$ ,  $\frac{\epsilon}{\epsilon_c} = 1.0$  and  $\frac{\epsilon}{\epsilon_c} = 3.0$ . The figure displays the enhancement of the flux at  $\theta \neq 0$  as a result of the superposition of radiation from source points off axis.

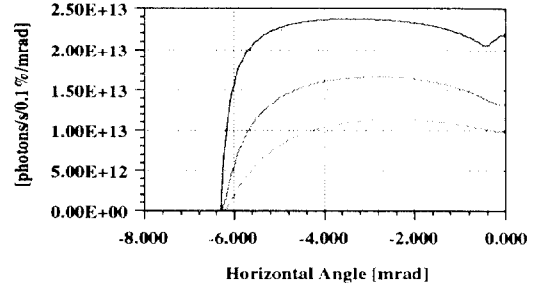


Figure 2: Photon flux as a function of horizontal angle corresponding to four photon energies shown from upper to lower curve  $\frac{\epsilon}{\epsilon_c} = 0.33$ ,  $\frac{\epsilon}{\epsilon_c} = 0.66$ ,  $\frac{\epsilon}{\epsilon_c} = 1.0$  and  $\frac{\epsilon}{\epsilon_c} = 3.0$ .

### 5.3 Polarization

The polarization is defined by the vectors of a given basis. In terms of the basis of circular polarization, the polarization rate is given by  $\rho_r = (I_r - I_l)/I_0$ , where  $I_r$  and  $I_l$  are the intensities of right and left circular polarization and  $I_0$  is the total flux. Figure 3 shows the general trend of flux and circular polarization verses photon energy at  $\theta = 0$ .

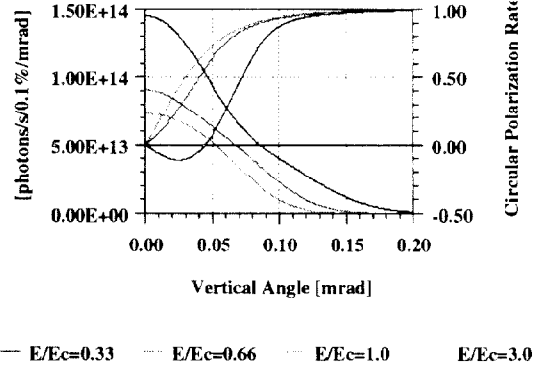


Figure 3: Circular polarization rates and photon flux as a function of vertical angle at four photon energies,  $\frac{\epsilon}{\epsilon_c} = 0.33$ ,  $\frac{\epsilon}{\epsilon_c} = 0.66$ ,  $\frac{\epsilon}{\epsilon_c} = 1.0$  and  $\frac{\epsilon}{\epsilon_c} = 3.0$ .

The circular polarization increases at higher photon energies where a compromise has to be made with angular flux. From the figure, the effect of enhanced flux at low photon energies can be seen to slightly decrease the circular polarization rate. At photon energies approaching  $\epsilon_c$ , however, the circular polarization is fully restored.

## 6 REFERENCES

- [1] J.A. Overweg, private communication.
- [2] M. Stampfer, Ph.D. Thesis, ETH Zürich, in preparation.
- [3] P. Elleaume, EPAC92, Berlin, Editions Frontiers (1992).